Available online at www.pelagiaresearchlibrary.com

Pelagia Research Library

Advances in Applied Science Research, 2014, 5(5):148-164

ISSN: 0976-8610
CODEN (USA): AASRFC

AVO analysis of 3-D seismic data at G-field, Norway

Fredrick Ogochukwu Okocha and Edmund Atakpo

Department of Physics, Delta State University, Abraka

ABSTRACT

The Amplitude variation with offset (AVO) analysis looks at how the amplitude of reflection events, such as those at the top of reservoir intervals, change with varying offset or reflection angle. By modelling these effects for different reservoir fluids via fluid substitution, effects of production can be recognised within the seismic data. Amplitude differences viewed between survey vintages can also highlight the movement of fluid contacts and changing fluid compositions throughout the reservoir. AVO analysis was performed on the three wells; well A, B and C. The analysis involves in creating a synthetic model to infer the amplitude responses observed at a particular reservoir horizon. Four types of fluid model substitution were created; pure brine, pure oil, pure gas and brine mix (70% Brine, 20% Gas and 10% Oil). Prominent amplitude changes which correspond primarily to the production effects can be seen in the Tarbert reservoir.

Keywords: Amplitude variation with offset (AVO), fluid substitution, synthetic model, Tarbert reservoir)

INTRODUCTION

The G-field is located on the western offshore of Norway as illustrated in Figure 1. This field is a part of the northern North Sea oil and gas field and is currently operated by Statoil. The field was first spudded in the late 1970s, and began its oil production in the late December of 1986 [1]. It was estimated that this field bears recoverable reserves amounting to 319 MSm^3. This amount corresponds to about 20 Mbbl of recoverable reserves. However, as of 31st December 2011, a new estimate for the recoverable reserve was calculated. About 365 MSm^3 of recoverable reserves was found [1].This new estimate reflects a significant progression in the reservoir development. In fact, it was through the onset of passive drive mechanisms such as water injection for improved oil recovery and through the application of time lapse seismic reflection survey (or 4D seismic) for continuous monitoring of the field, that has significantly improved the understanding of the fluid distribution in the reservoir. Furthermore, it has been estimated that about 14 MSm^3 of reserves still remains in this field which require the implementation of improved recovery methods and monitoring. The need to monitor the reservoir is indeed crucial and thus the application of amplitude versus offset analysis is needed.

Selected vintages of the G-Field seismic data sets (1985 3-D, 1999 3-D and 2003 3-D) were analysed for amplitude variations with offsets. The objective of this study was to determine whether amplitude variation with offset (AVO) analysis could confirm the interpretation of bright spots as determined from amplitude anomalies delineated on the 3-D data volumes. Amplitude anomalies observed in the three vintages are interpreted to be caused by the effect of fluid and pressure changes to seismic amplitudes.

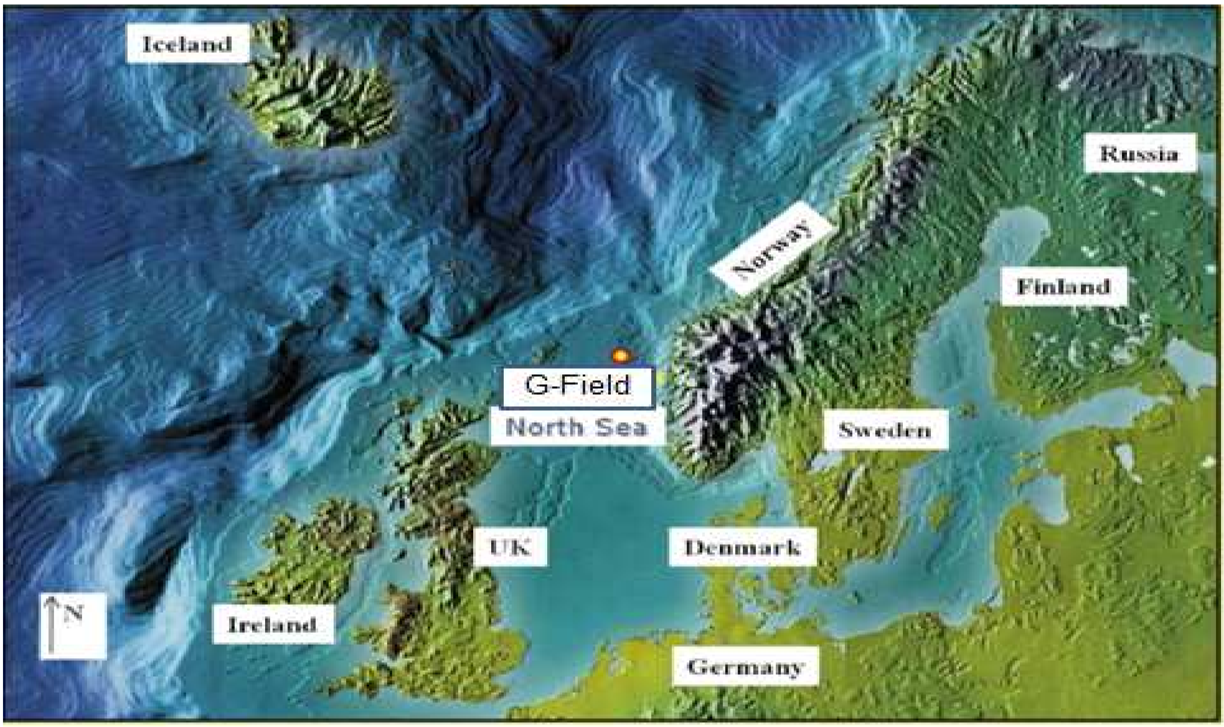

Figure 1: The location of the G-field

Geological Settings of G-Field

The G-field is structurally deformed. It is a rotated domino fault block system [2] as shown in Figure 2. The evolution of this field occurred mainly between late Jurassic to early Cretaceous period although some have documented that the rifting phase of the Permian-Triassic age to some extent probably have influenced the structural complexity seen in this field [3]. As a result, the reservoirs are highly compartmentalized and not laterally continuous.

There are three main separate reservoirs found within the G-field; the Brent group, the Cook formation and the Lunde-Statfjord formation. The Lunde-Statfjord formation is the oldest and the Brent group is the youngest. The reservoir interval from the Lunde-Statfjord formation comprises of alterations of mud, shale and sand of semi-arid fluvial to alluvial environment. The reservoir quality in this formation is classified as moderate to very good; it is generally an oil bearing reservoir [3]. The next reservoir is from the Cook formation. It is an oil bearing reservoir although some presence of proven gas was documented in the past [3]. The Cook formation is a part of the Dunlin group and it comprises of mainly muddy and sandy shale of marine, shoreface and marginal estuary setting. The reservoir quality is generally classified as moderate to good quality. The influence of high permeability regions present in the Cook formation may have influenced the migration of hydrocarbons. The next reservoir section is the Brent group. It is divided into four formations; Tarbert formation, Ness formation, Etive formation and Rannoch formation. The Brent group is the largest contributor to the amount of recoverable reserves found within the G-field [3]. It comprises of mainly deltaic sandstones with good to very good reservoir quality. The Brent group reservoir is oil filled with an initial gas cap. The reservoir communication is non-continuous as the presence of faulted blocks lead to complex flow pattern. A notable unconformity which can be seen from a seismic section represents the base Cretaceous. This unconformity remains the dominant regional cap rock to this field. Local seals, those relating to lithological changes and structural deformities such as faults and intercalations of impermeable rock layers, are present though large accumulations of hydrocarbons were mainly found below this stratigraphic unconformity. The main source rock for this field is the Draupne formation although for the Brent group, the source rocks are from Draupne and Heather formation [2]. Both are of base upper Jurassic to base lower Cretaceous.

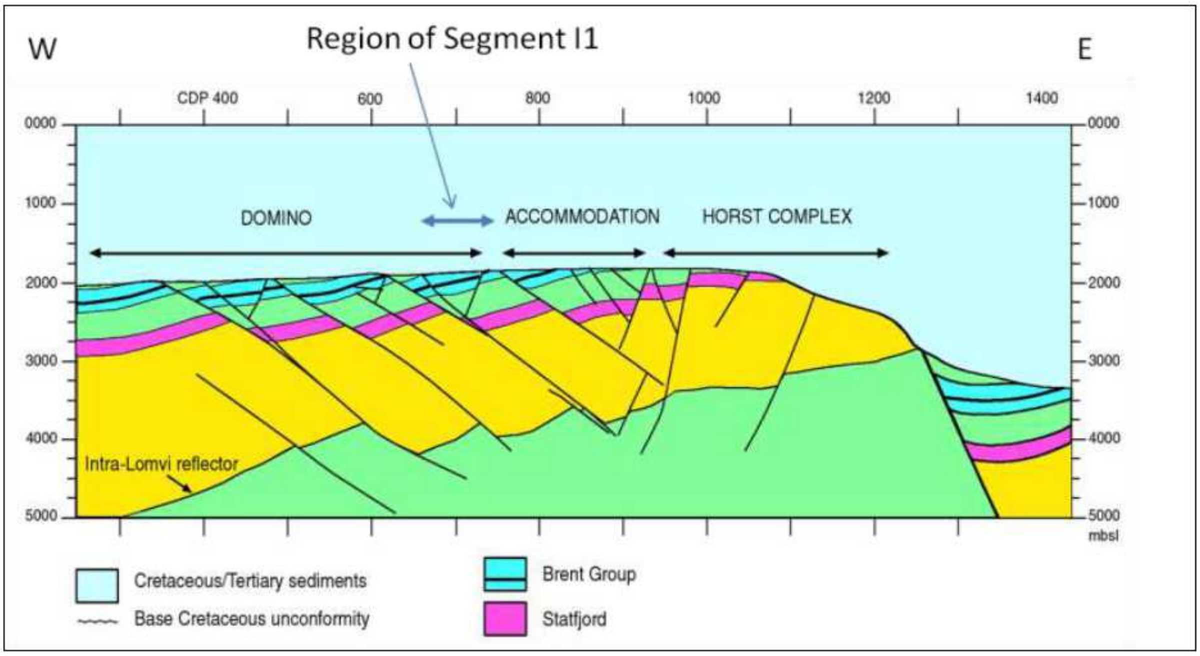

Figure 2: Complex structural deformities primarily defined by normal faulting due to extensional rifting

AVO METHODOLOGY

AVO technique is the analysis of the variations of the amplitude as a function of offset. The amplitude varies with offset because the reflection coefficient varies when the angle of incidence of the wave at the interface varies [4]. These variations are governed by the contrast in *P*-wave velocity and *S*-wave velocity at the interface. When there is gas in the layer, V_p drops whereas V_s does not change. This means that V_p/V_s is anomalous, and we hope to see the effect of this anomaly in the reflection pattern. In principle AVO analysis should measure amplitude variations with angle of incidence. However, amplitude is measured with offset because usually as offset increases, the angle of incidence increases. We also assume that amplitude of the seismic data is proportional to the reflection coefficients [5]. By modelling the AVO effects for different reservoir fluids, AVO responses in seismic data can be predicted.
The AVO response is dependent on three parameters; the P-wave velocity, the S-wave velocity and the density in a porous reservoir rock. Density is relatively simple to model as its behaviour with changing water saturation is linear and can be found using the equation below

$$\rho_{sat} = \rho_m(1-\varphi) + \rho_w S_w \varphi + \rho_{hc}(1-S_w) - (1)$$

Where ρ is density (saturated, matrix, water, hydrocarbon), S is saturation and Φ is porosity

However, in reality, these equations do not entirely correctly describe the wave propagation in rocks that are saturated with fluid. The values for density, bulk modulus and shear modulus need to be replaced with those adapted for the saturated rock, which can be done by using the Biot-Gassmann equations [6]. Varying the fluid content of the reservoir rock can produce noticeable AVO effects. Fluid substitution is carried out to model the effect that different fluids or combinations of fluids will have on the amplitude response. The Biot-Gassman equations allow for the original in-situ fluid to be ‘removed’ from the rock and another fluid or fluid combination to be put in its place.

The Biot-Gassman Equations allow the density, P-wave and S-wave velocity equations to be updated to take into account the dry and saturated rock cases. As these equations contain a bulk modulus value (the inverse of compressibility), an expression is required to calculate the saturated bulk modulus [7].

$$K_{sat} = K_{dry} + \frac{\left(1-\frac{K_{dry}}{K_m}\right)^2}{\frac{\varphi}{K_{fl}} + \frac{1-\varphi}{K_m} - \frac{K_{dry}}{K_m{}^2}} \quad ----(2)$$

Where sat = saturated rock, dry = dry frame, m = rock matrix, fl = fluid and Φ = porosity

In order to substitute or replace the fluids in the target reservoir for modelling, the density, P-wave velocity and S-wave velocity logs are required. By use of the Biot-Gassman equations, these logs can be converted to how they would appear for whichever fluid effect is being modelled. These logs can be seen in Figure 3. In the case of the G-field data, there was no need to calculate an S-wave velocity log as this was already available from the well data.

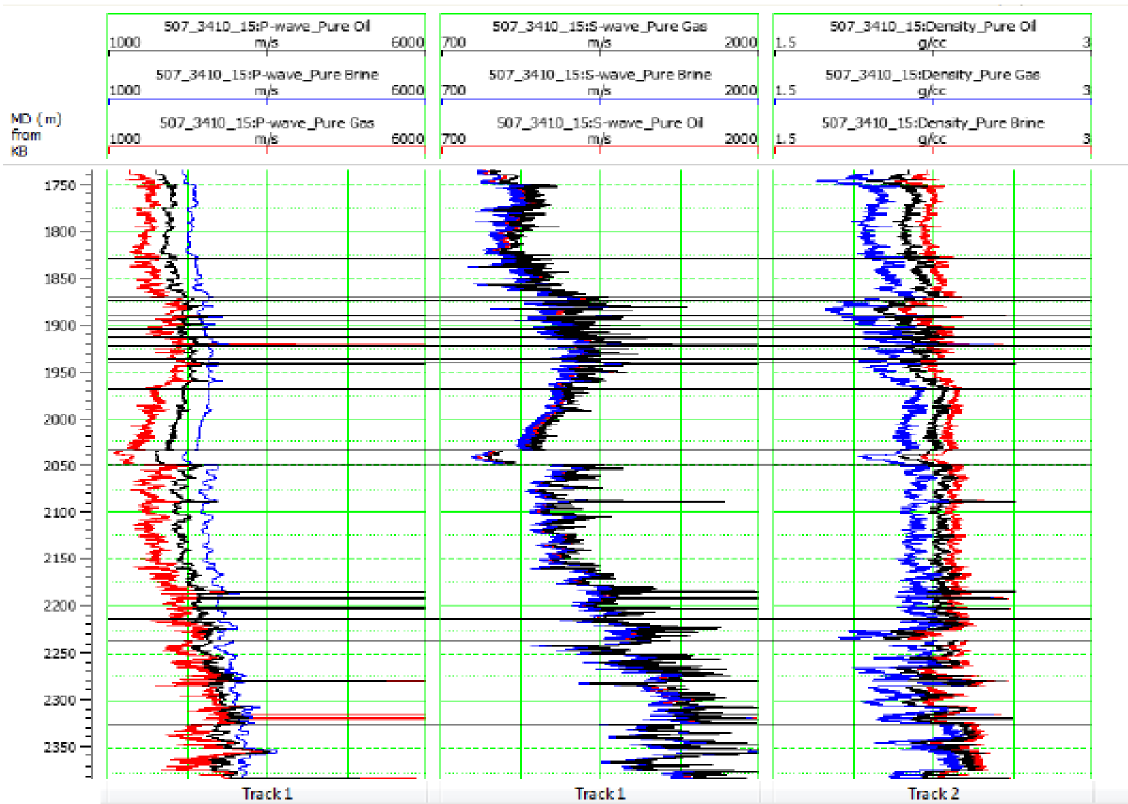

Figure 3: Log curves for density, P-wave velocity, S-wave velocity and Poisson Ratio for pure brine, pure oil and pure gas cases for Exploration Well B

AVO MODELLING OF THE G-FIELD DATA

In AVO analysis, the Zoeppritz equations are used to extract S-wave type information from P-wave reflections at different offsets/angles. In the analysis of the G-field data, an approximation to the Zoeppritz equations called the Aki-Richards equations is used. The two-term version of this equation was selected; these two terms, A and B, representing the intercept and gradient of the AVO curve respectively [8].

The Aki-Richard equations are used along with a source wavelet extracted from the seismic data to form synthetics. These synthetics can be modeled for pure brine, pure gas, pure oil cases or cases with a combination of these fluids. The source wavelet was estimated by extracting a statistical wavelet from the Pre Stack Time Migrated (PSTM) seismic data collected in 1985. This wavelet was also rotated 180 degrees to match with the European polarity convention for the G-field data. The wavelet can be seen in Figure 4

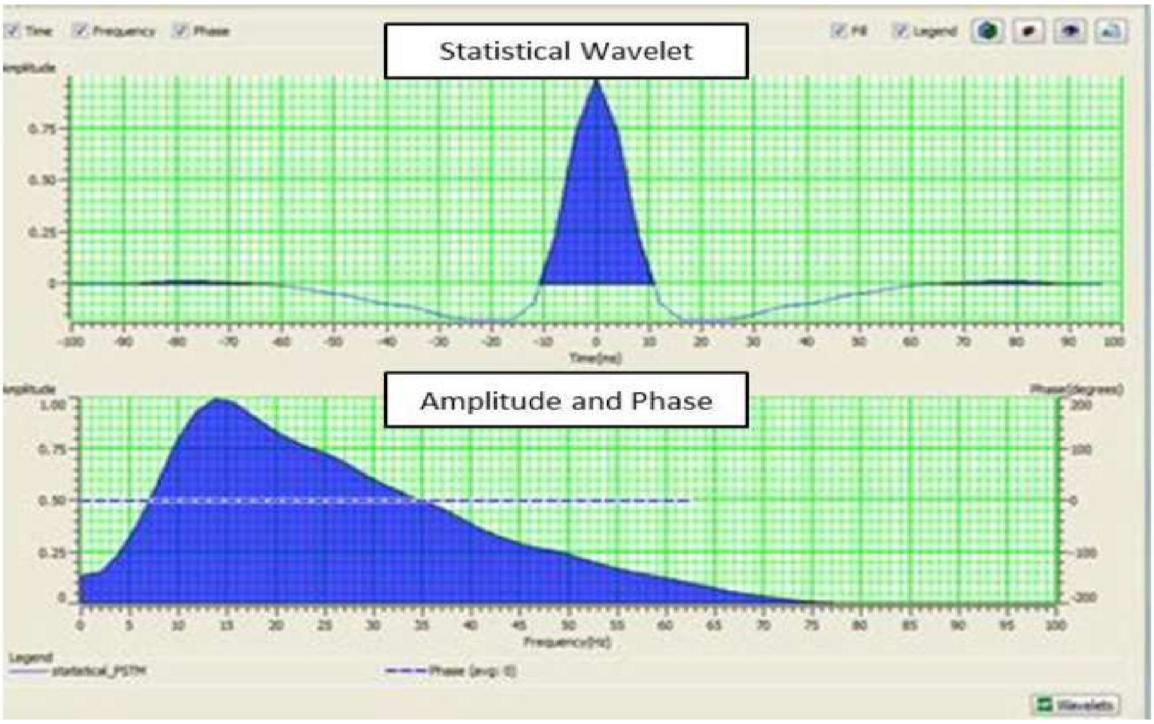

Figure 4: Statistical wavelet extracted from the 1985 vintage PSTM seismic cube

As this data has been time migrated, it contains less noise than the near, mid and far offset data. A wavelet was extracted from one of these data sets for comparison and can be seen in Figure 5

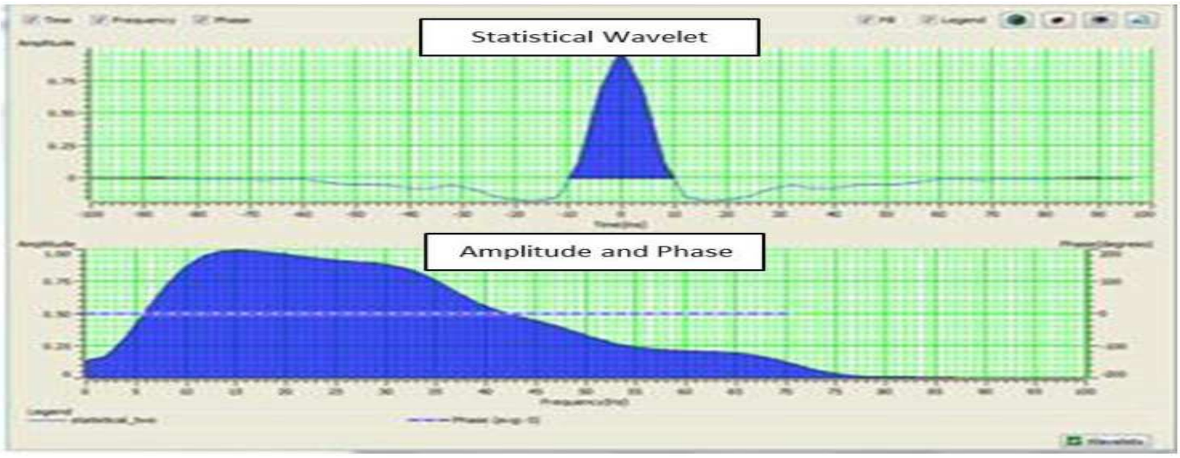

Figure 5: Statistical wavelet extracted from unmigrated seismic data demonstrating the fact that it is noisier than the wavelet seen in the previous figure

Synthetic traces are calculated using the velocity and density logs as well as depth-time data and the wavelet that was extracted. It can be checked how well the synthetic matches the seismic data by examining their cross correlation. This correlation process will also suggest whether the synthetic should be shifted in time to match better with the seismic data (Figure 6)

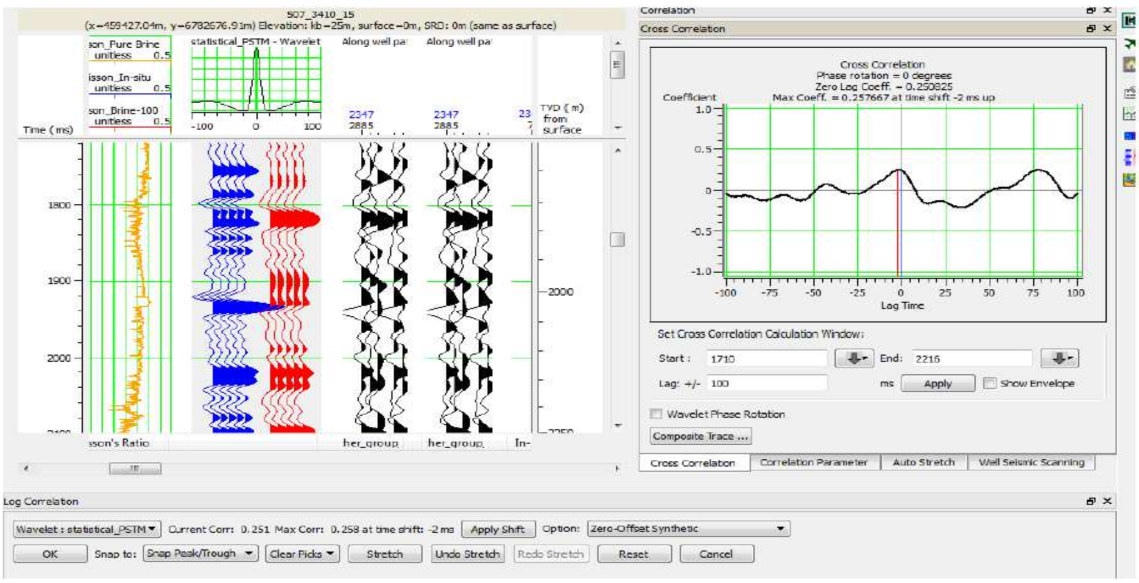

Figure 6: Demonstrating cross correlation between the synthetic and seismic data. The red traces are extracted from the seismic data at the well location and the blue traces are copies of the synthetic trace. The plot of the right shows the correlation coefficient between the two sets of traces plotted against lag time. It also gives a suggested time shift to apply so that the traces match optimally.

Sets of synthetics for different fluid cases can then be generated using the altered logs calculated by fluid substitution (Figure 7)

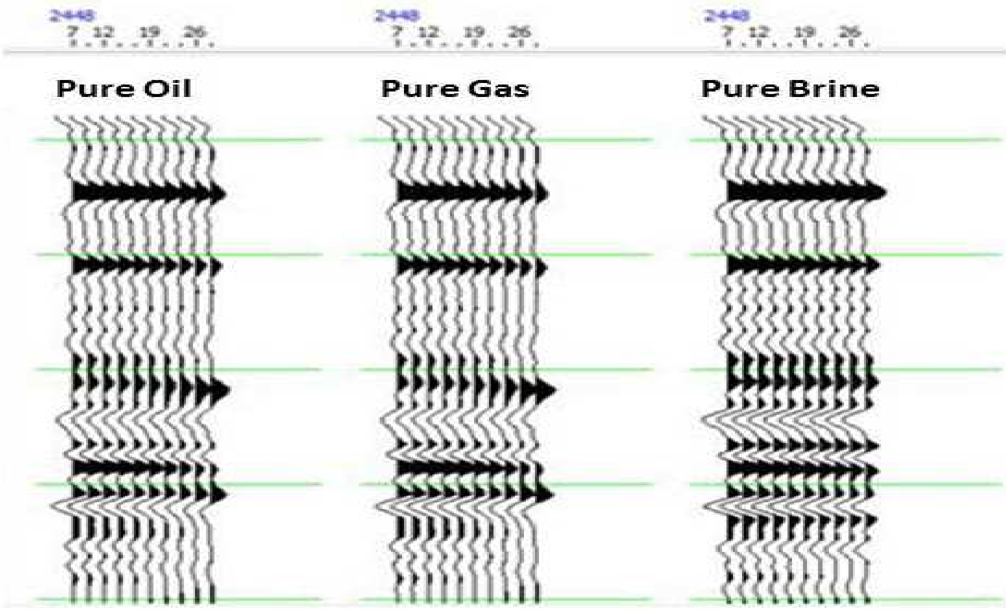

Figure 7: Synthetics for pure brine, pure oil and pure gas cases modelled at the location of well B

Converting from Offset to Angle

For each of the vintages (1985, 1999, 2003) there are near, mid and far offset stacked data. By calculating the average reflection angle for each of these offsets, it is possible to create angle gathers. In the angle gather, each trace corresponds to a constant incidence/reflection angle [9].

Using the acquisition parameters and basic geometry, the reflection angles can be calculated for the near, mid and far offset data.

288 channels with a spacing of 12.5 m give a total active cable length of 3600 m. The shot interval is 18.75 m and as the shots were done flip-flop (one source fired, then the other) making the interval for any subsurface line 37.5 m.

The shot interval is three times that of the group interval making the fold one sixth of the number of channels (288/6 = 48). Each CMP gather therefore has 48 offsets and these have been divided into three equal groups of 16. An average depth to reservoir was used of 2860 m. The acquisition geometry and angles for the offsets can be seen in Figure 8.

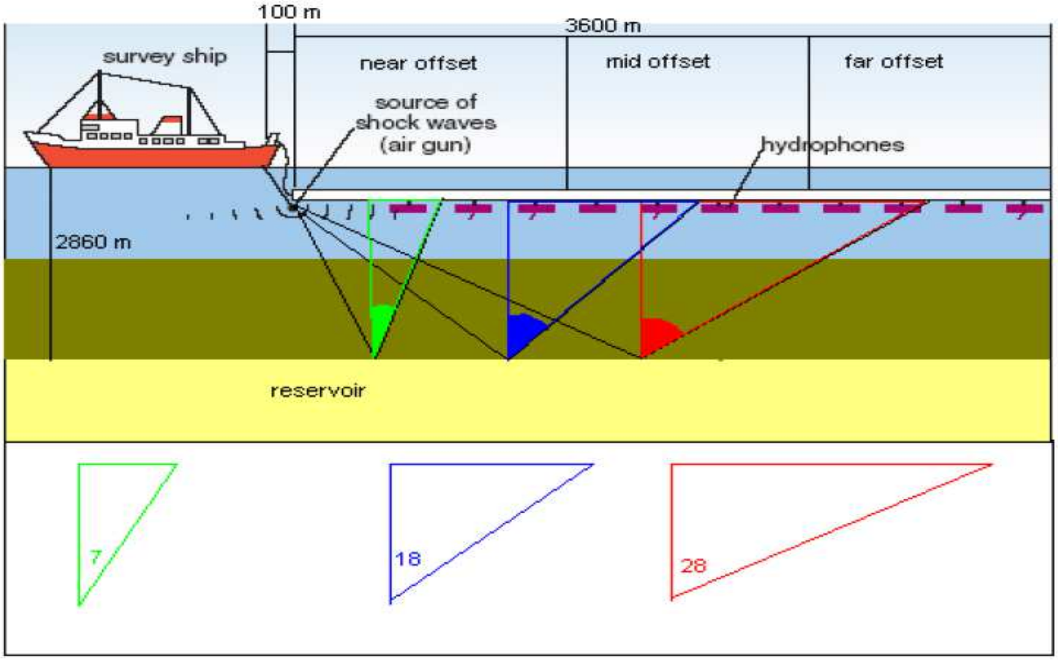

Figure 8: Demonstrating the geometry used to calculate the near, mid and far offset reflection angles shown in green, blue and red respectively

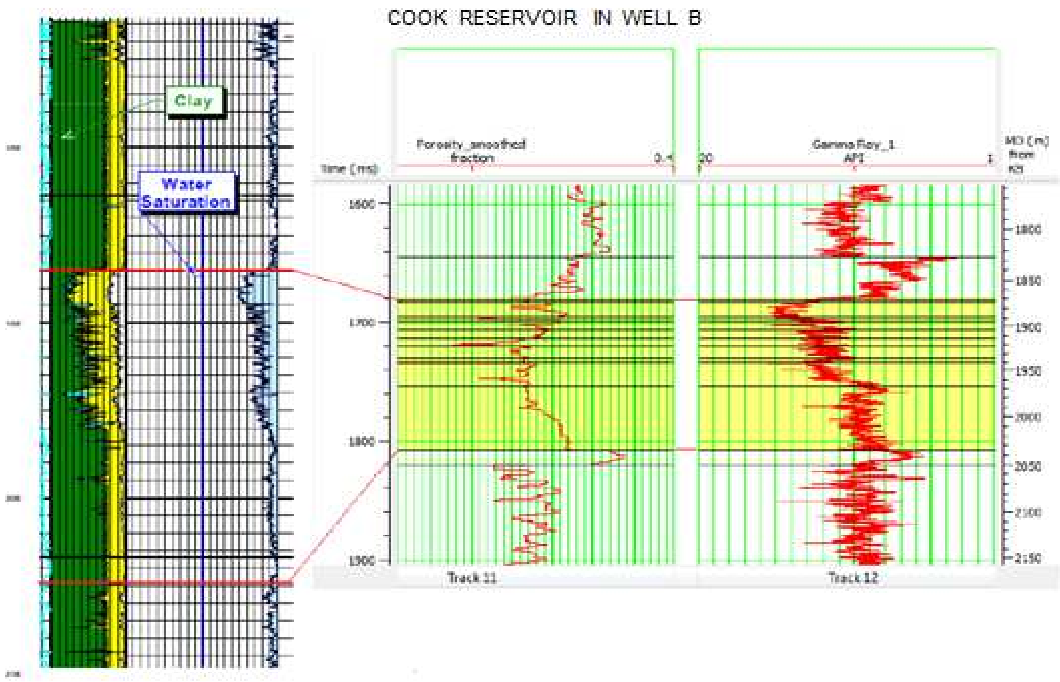

Figure 8: Well log for well B demonstrating why this well was chosen for the Cook reservoir interval as it is easily recognised by the higher porosity and lower gamma ray (due to fewer radioactive materials in a clean sandstone relative to a shale) as well as a higher water saturation and lower clay content (seen on left)

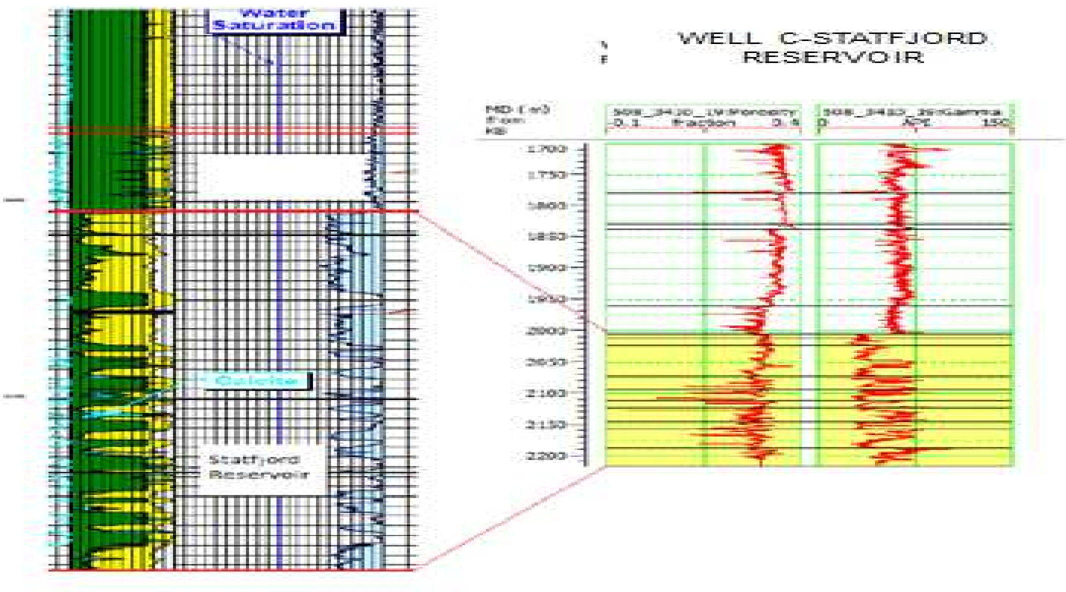

Figure 9: Well C logs showing the location of the Statfjord Reservoir interval. This can be identified by low gamma ray response, higher porosity and a lower clay fraction (show in green in the left log)

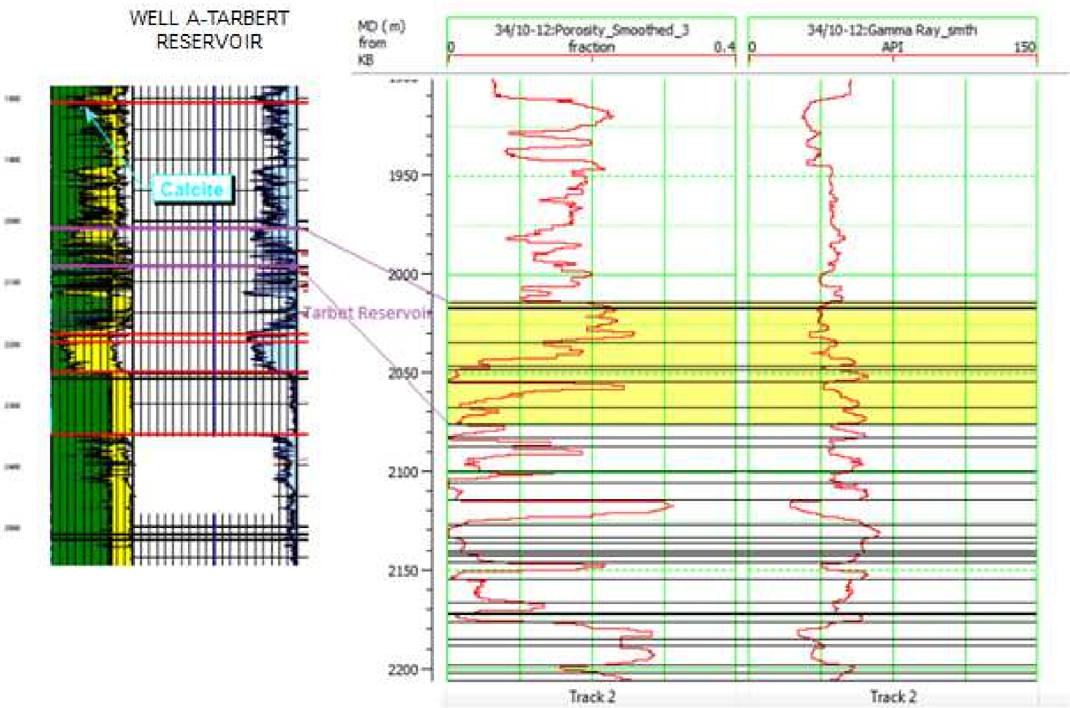

Figure 10: Well A logs showing the location of the Tarbert reservoir interval. Higher porosities can be identified at the top of this interval (central log) as well as lower gamma ray values than the interval above (far right log)

Selection of reservoir intervals and wells

The wells with logs available for use in interpretation are wells A, B and C in the G- field. Well B cuts through the Cook reservoir and this reservoir unit can be clearly identified from logs. For this reason, data from this well has been used to study AVO effects for the top of this reservoir unit (Figure 8). Well C cuts through the Statfjord reservoir, which can also be identified in the well logs. For this reason, data from this well has been used to study AVO effects for the top of this reservoir unit (Figure 9). In a similar manner Well A cuts through the Tarbert reservoir and data from this well has been used to study AVO effects for the top of this reservoir unit (Figure 10)

RESULTS AND DISCUSSION

The AVO effects were modelled for the Tarbert, Cook and Statfjord reservoirs for pure brine, pure oil and pure gas cases. An additional case with a mixture of fluids (70% brine, 20% gas and 10% oil) was modelled in the Tarbert reservoir as this fluid composition is a better representative of that which might be found in areas of production. By modelling its AVO effect, a similar response can be searched for within the seismic data to indicate the presence of such fluid changes.

Statfjord Reservoir (Well C)

For each reservoir, the correlation between the synthetic and seismic data was tested to see how well they matched. This shows whether it is reasonable to use the AVO effects seen in the models to look for the same effects within the seismic data. Figure 11 shows the correlation between the synthetic and the seismic data for Well C.

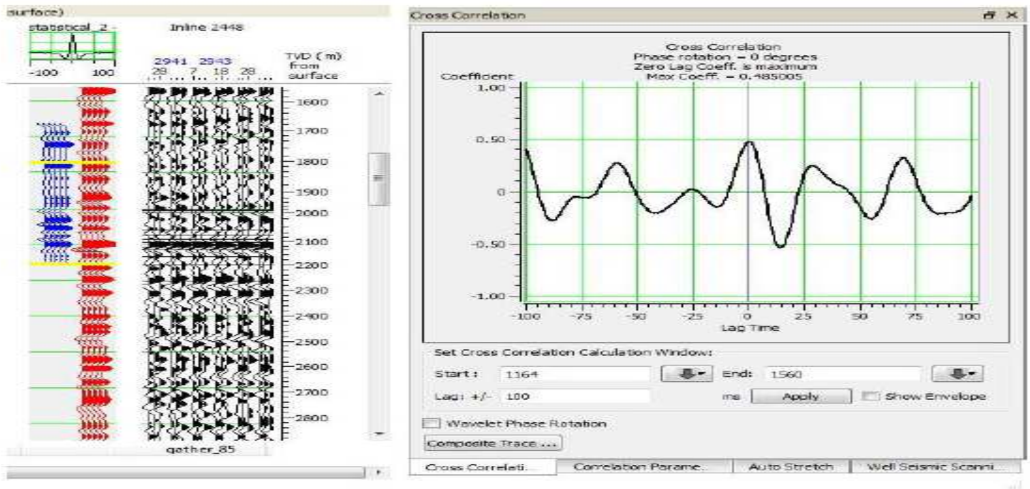

Figure 11: correlation between the synthetic and the seismic data (well C, '85 vintage) The blue curves represent the synthetic, the red is a repeated trace extracted from the seismic at the well location. The black curves are the '85 vintage angle gather. The correlation is almost 50%

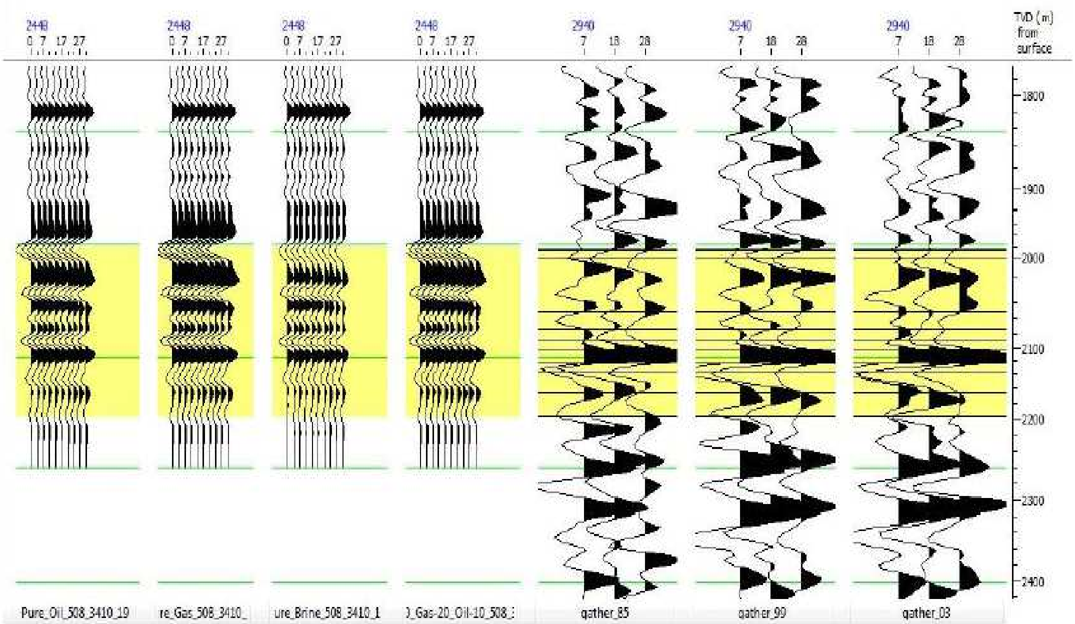

Figure 12: synthetics (left to right) generated for pure oil, pure gas and pure brine and a 70:20:10 (brine:oil:gas) ratio scenarios. The Statfjord reservoir is shown in yellow. The traces on the far right show the seismic data (from left to right: angle gather '85 vintage, '99 vintage and '03 vintage) for comparison

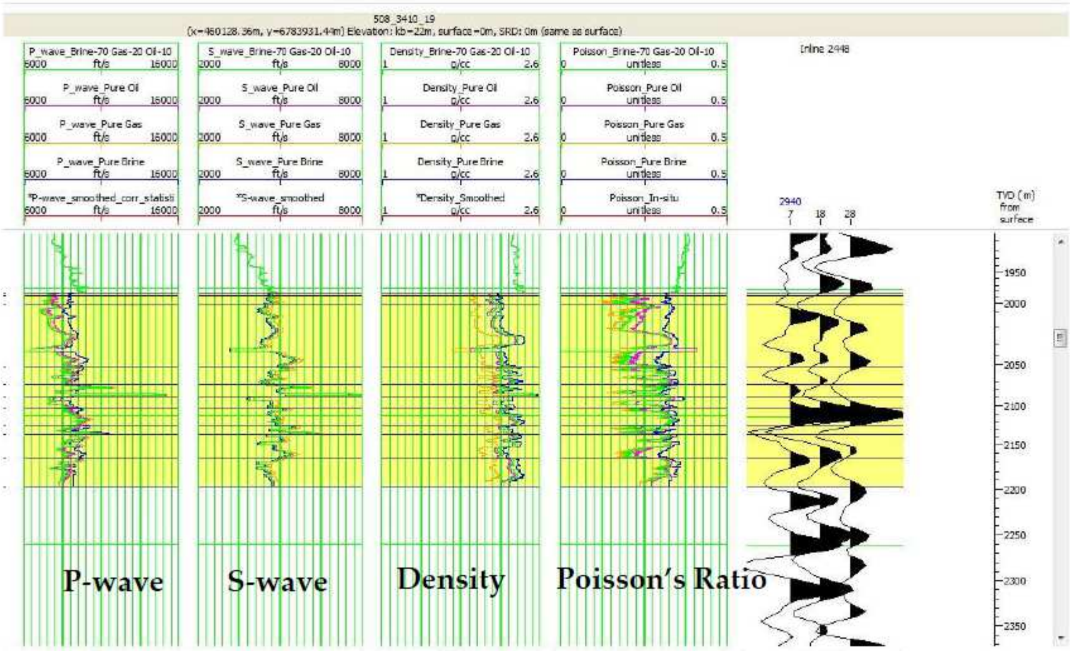

Figure 13: P-wave, S-wave , Density and Poisson ratio curves for the pure brine, pure oil, pure gas and 70:20:10 (brine:gas:oil) scenarios. Statfjord reservoir marked on in yellow. Logs are from well C

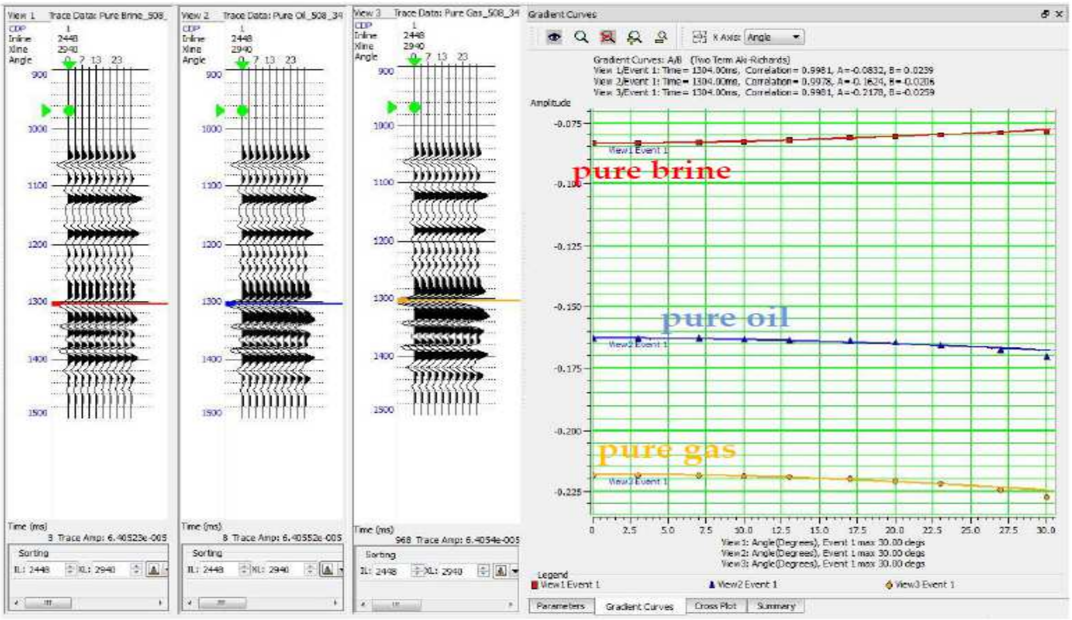

Figure 14: AVO gradient analysis for well C (focusing on Top Statfjord reservoir) for the pure brine (red), pure oil (blue) and pure gas (yellow) cases with the corresponding synthetics shown on the left

Synthetics were then generated for the different fluid cases and can be seen in Figure 12. The P-wave, S-wave and density logs used to generate the synthetics can be seen in Figure 13. The AVO response was then modelled for the top of the Statfjord reservoir unit at the boundary between the shale and porous sand (Figure 14). Going from the pure brine to pure oil to pure gas cases, the intercept and gradient both decrease as is expected for the addition of hydrocarbons. As the negative amplitude increases, it will appear to brighten in the seismic data. The intercept-gradient cross-plot (Figure 15) shows how the data for the brine case lies on the wet trendline and that for the pure oil and pure gas move off this trendline into the top of the lower left hand quadrant denoting a class III low impedance sand, which is expected for the G- field

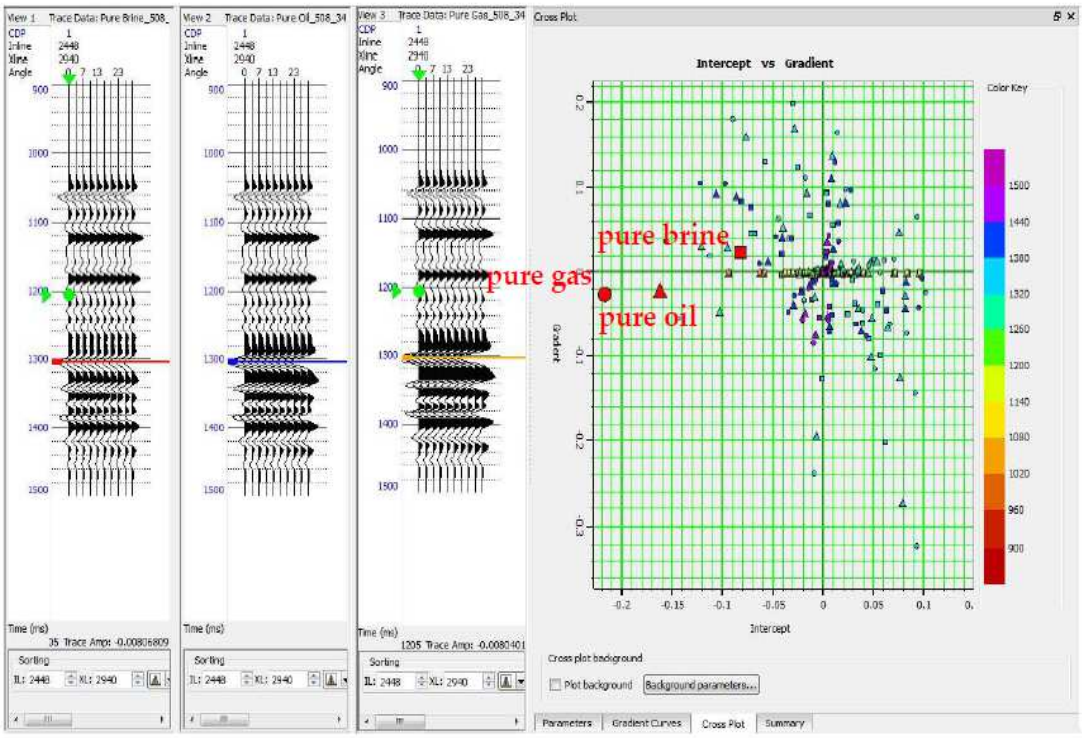

Figure 15: crossplot of Intercept vs Gradient (well C - Top Statfjord) for the pure brine (square), pure oil (triangle) and pure gas (circle) cases

Well B- Cook Reservoir

The same analysis was carried out for the Cook reservoir using data from well B. Figure 16 shows the cross correlation between the synthetic and the seismic data at this well and Figure 17 shows the logs used in the fluid substitution used to create the synthetics to model the different AVO fluid effects

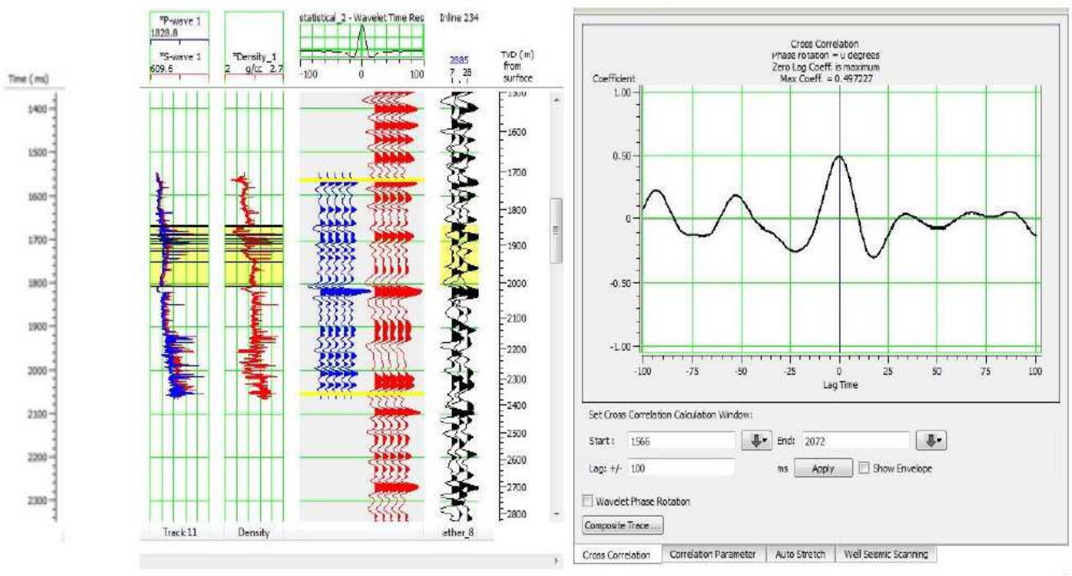

Figure 16: correlation for well B synthetic and '85 data. Correlation is around 50%

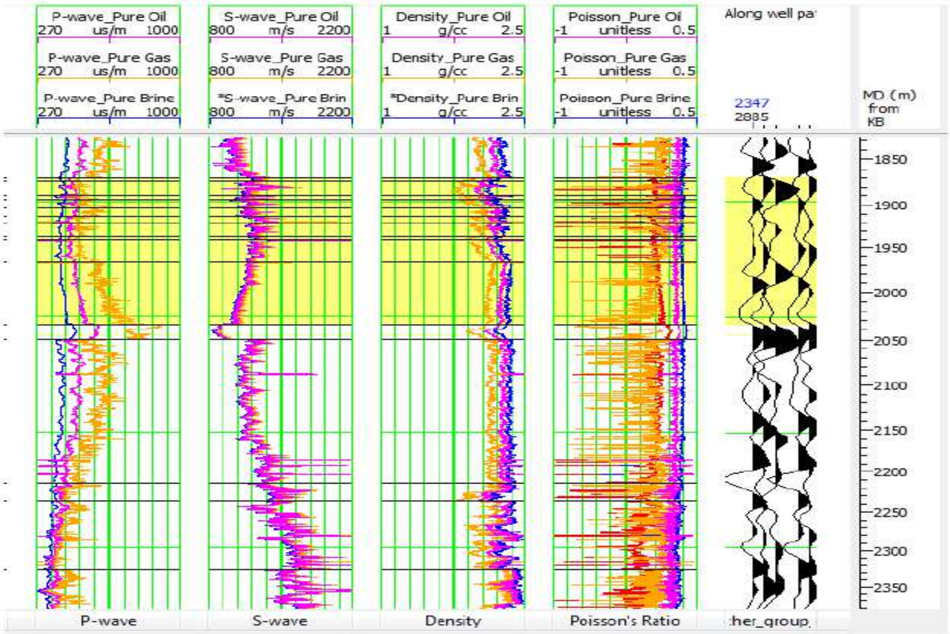

Figure 17: Well B - Cook Formation (yellow) - logs for pure brine, pure oil and pure gas cases used to calculate corresponding synthetics for these different fluid cases

Figure 18 shows the synthetics generated for this reservoir. The AVO plot (Figure 19) shows similar results as were found for the Statfjord reservoir with similar trends for the different fluid cases. The cross-plot (Figure 20) also gives similar results to the Statfjord reservoir with the pure oil and gas points moving off the wet trend and into the area corresponding to that expected for class III reservoir sand.

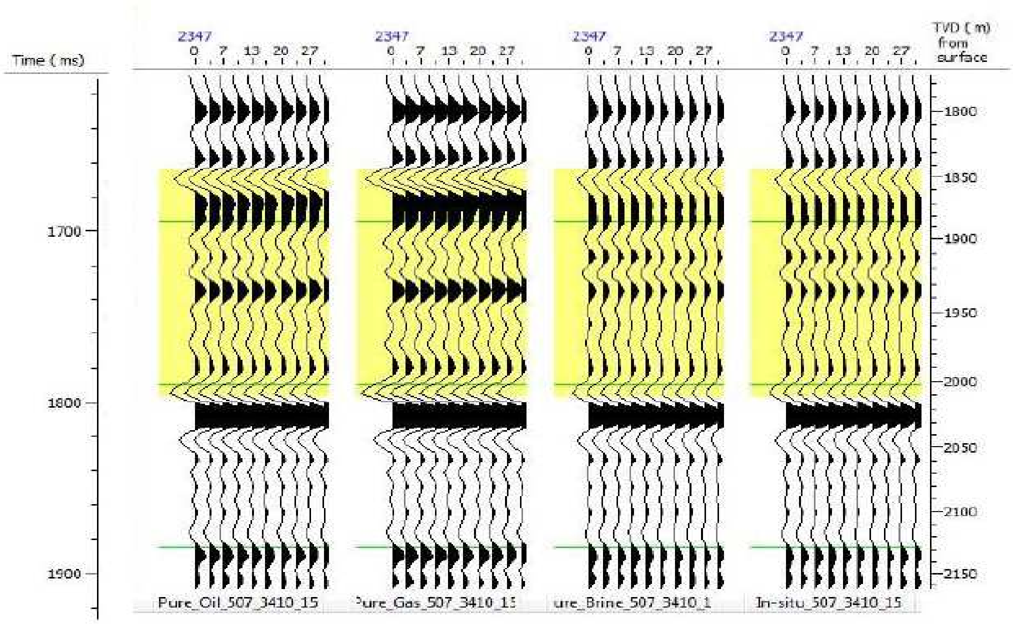

Figure 18: Synthetics for the Cook reservoir interval for pure oil, pure brine and pure gas case

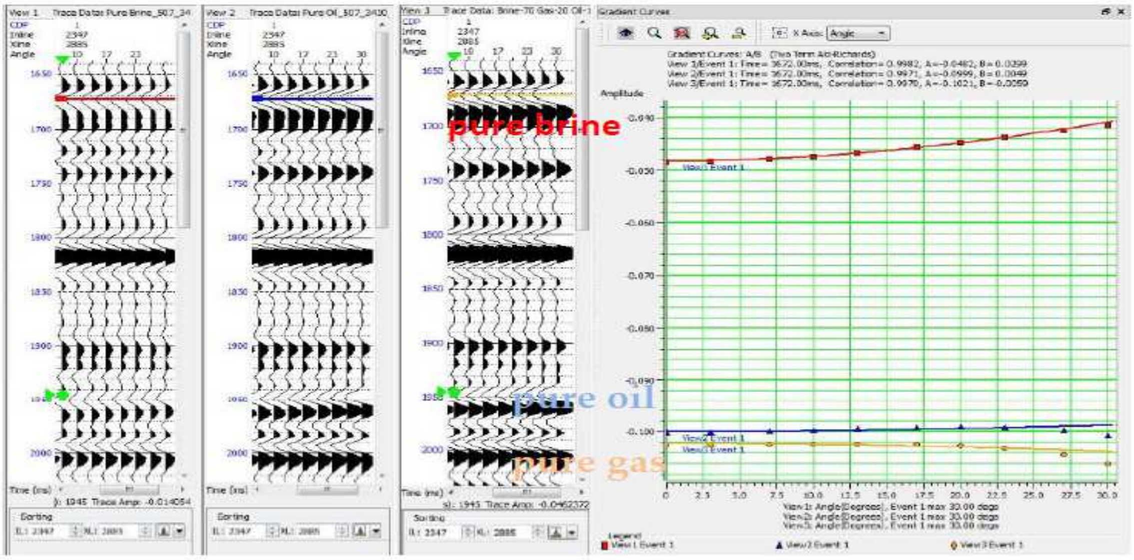

Figure 19: AVO plot for well B (Top Cook reservoir) for pure brine (red), pure oil (blue), pure gas (yellow)

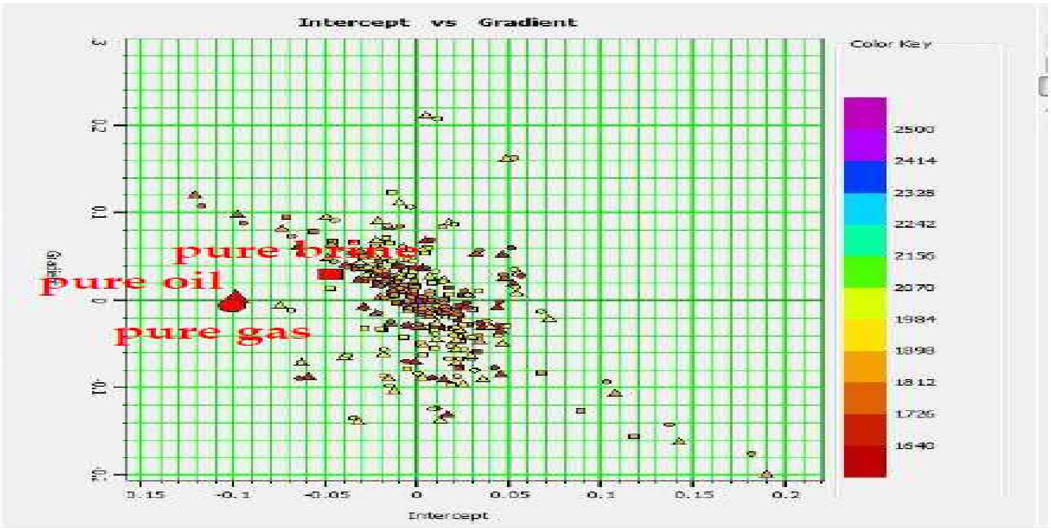

Figure 20: crossplot for the Top Cook reservoir (well B) for pure brine (square), pure oil (triangle) and pure gas (circle) cases

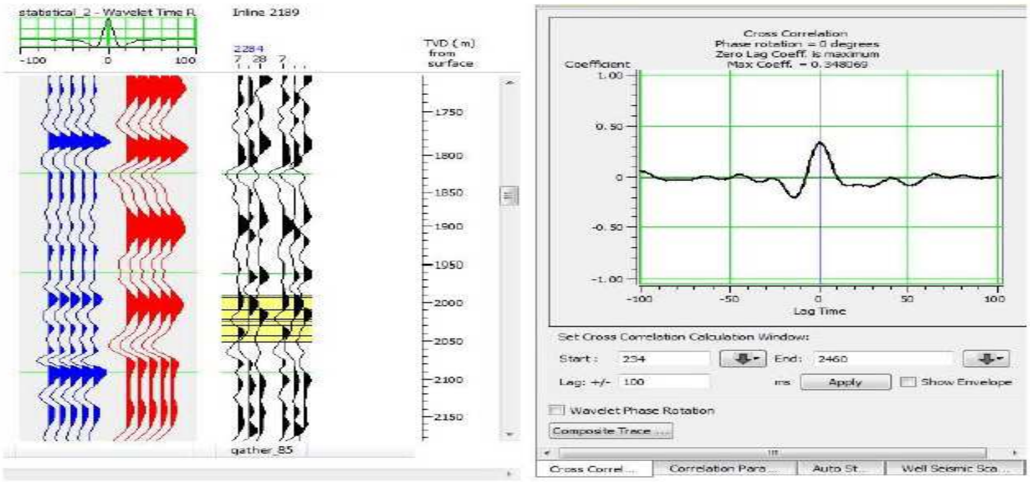

Figure 21: correlation between the synthetic and the seismic data (well A, '85 vintage) The blue curves represent the synthetic, the red is a repeated trace extracted from the seismic at the well location. The black curves are the '85 vintage angle gather. The correlation is around 30%

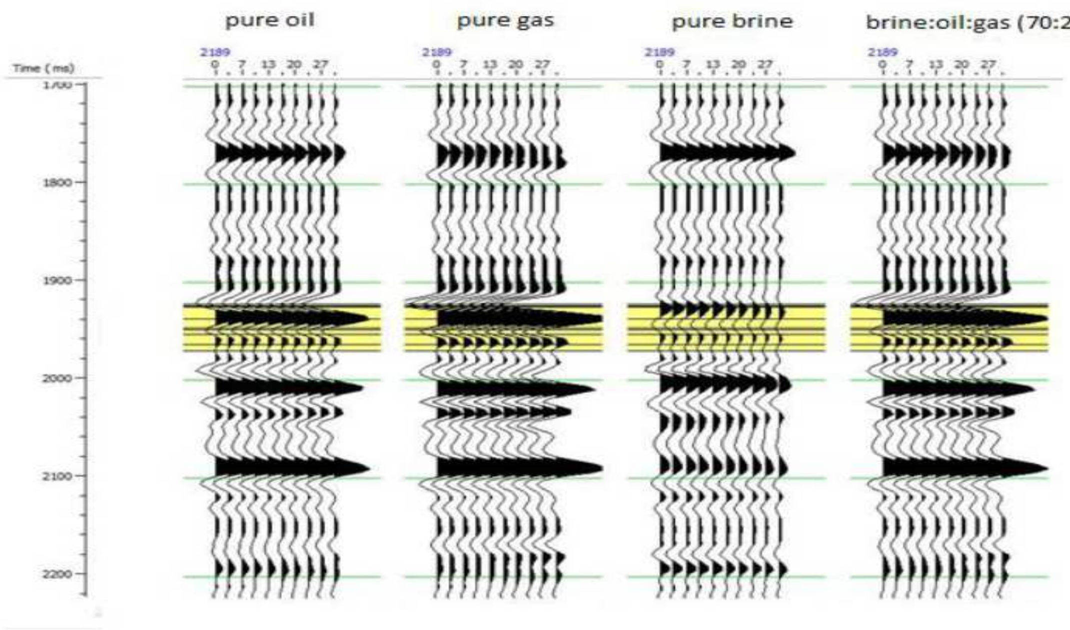

Figure 22: synthetics (left to right) generated for pure oil, pure gas and pure brine and a 70:20:10 (brine:oil:gas) ratio scenarios. The Tarbert reservoir is shown in yellow

Well A – Tarbert Reservoir

The same analysis again was applied to well B but with the additional model using a combination of fluids as this represents a more realistic situation expected in areas undergoing production effects. The correlation between the synthetic and the seismic data for this well can be seen in Figure 21 and the synthetics for all fluid cases in Figure 22.

The AVO plot (Figure 23) again demonstrates similar effects as seen for the previous two reservoirs but these are more pronounced. The brightening effect in the seismic data would be expected to be clearer for the top of this reservoir unit as shown by the steeper gradients. The cross-plot (Figure 24) shows how the points for the pure oil and the mixture of fluids have moved away from the brine trend to a greater extent than previous reservoirs. These stronger AVO effects suggest that the Tarbert reservoir is cleaner and more porous sand than the Statfjord and Cook reservoir. This agrees with porosity data ranges for the three reservoirs: Statford (24-28%), Cook (26-30%) and Tarbert (32-34%).

The Tarbert reservoir produced the strongest AVO effect in the models, even for the simulated reservoir fluid expected in production areas. For this reason, it was identified in the seismic data and the same AVO analysis applied at a location where production effects are expected. The AVO effect at the top Tarbert reservoir was looked at in the angles gathers of the 1985, 1999 and 2003 surveys.

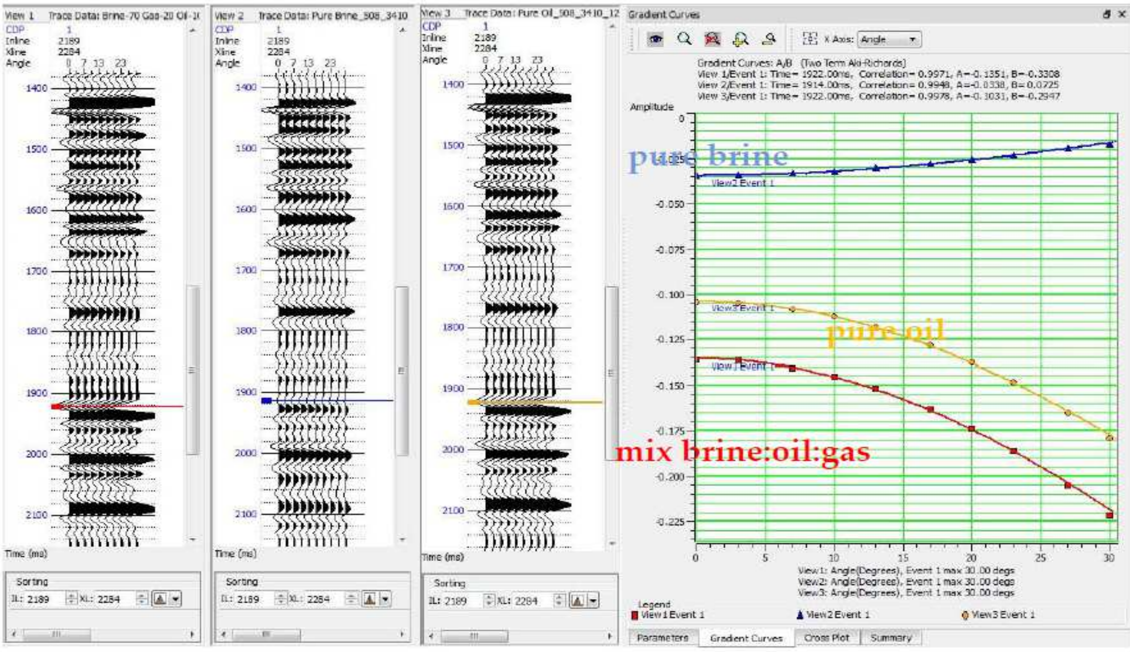

Figure 23: AVO plot for well A (focusing on Top Tarbet reservoir) for the pure brine (blue), 70:20:10 (brine:oil:gas) (blue) and pure oil (yellow) cases

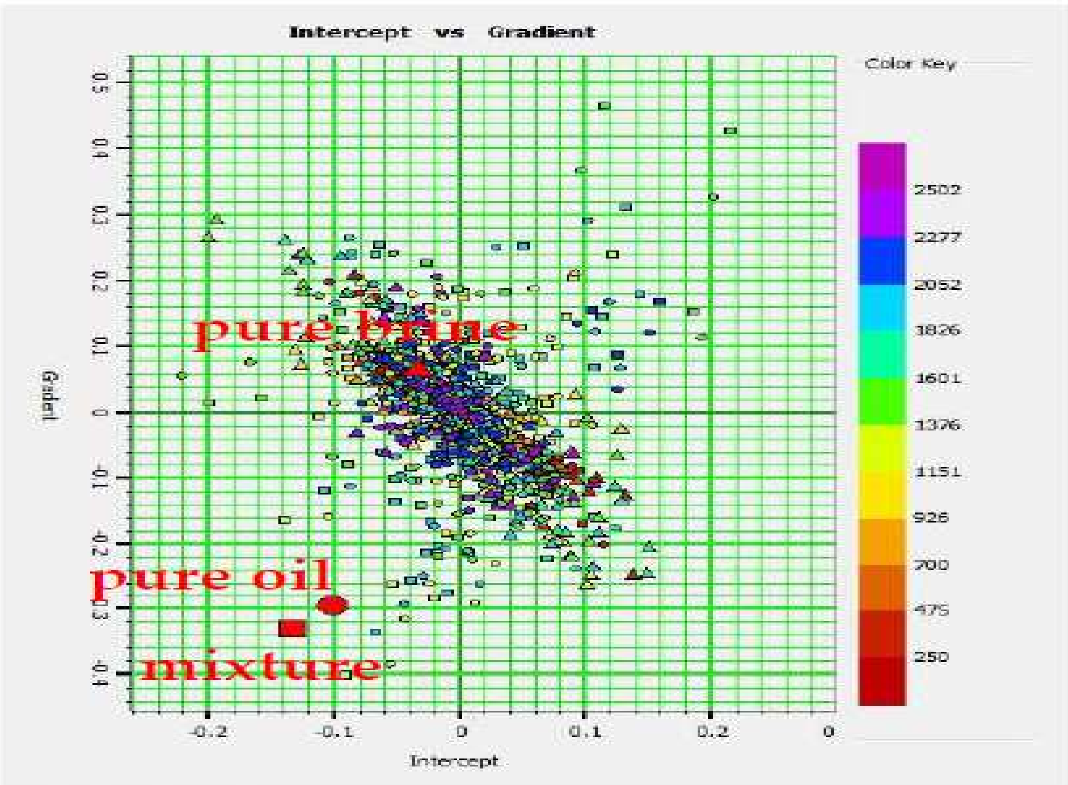

Figure 24: crossplot of Intercept v Gradient (well A - Top Tarbet) for the pure brine (triangle), pure oil (circle) and 70:20:10 (brine:oil:gas) (square) cases

Figure 25 and Figure 26 show the cross-plot and amplitude versus reflection angle respectively. The ’03 and ’85 surveys lie close to the brine trendline on the cross-plot whilst the ’99 survey has moved off the trendline suggesting the presence of hydrocarbons.

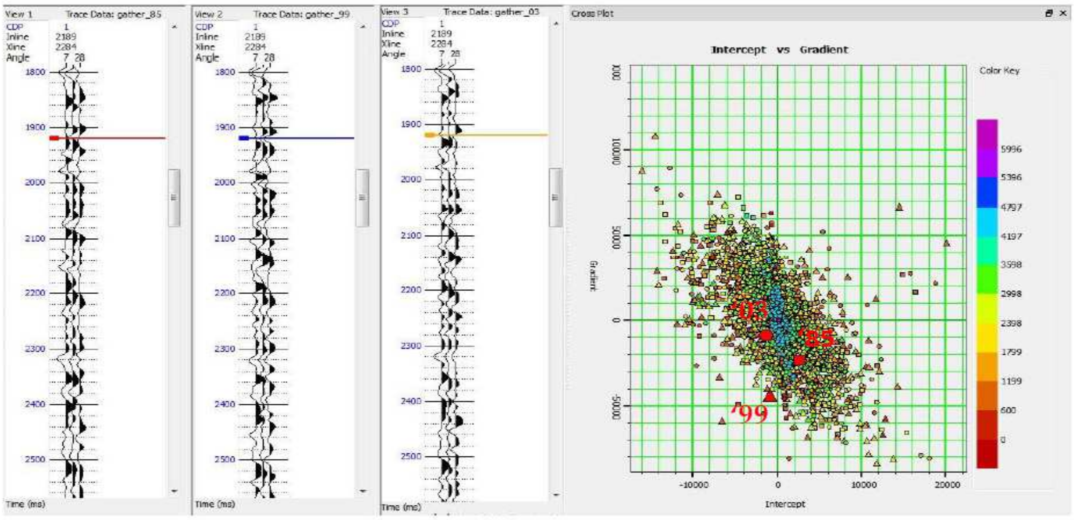

Figure 25: cross-plot of intercept vs Gradient (well A - Top Tarbert) for the '85 (square), '99 (triangle) and '03 (circle) angle gathers

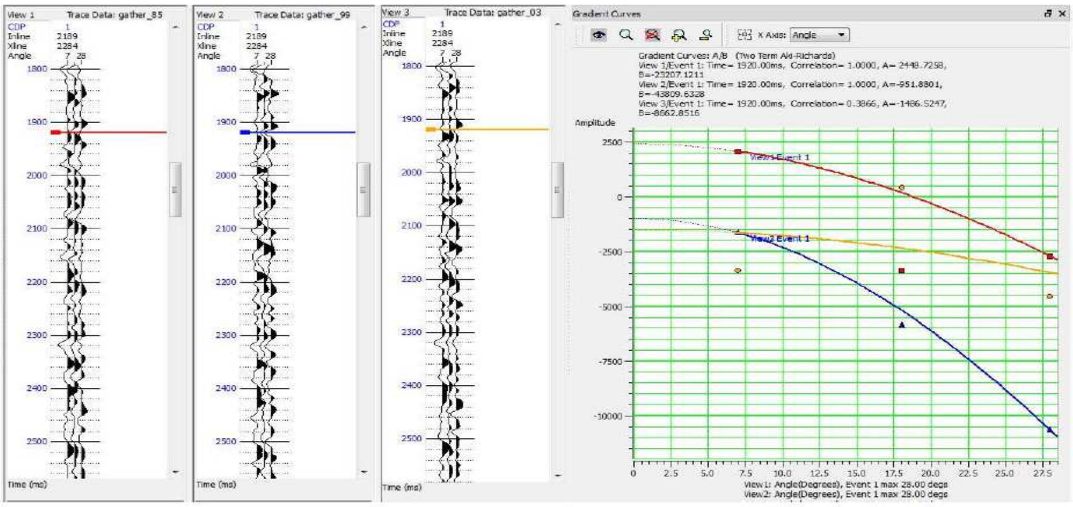

Figure 26: AVO gradient analysis for ’85 (red), ’99 (blue) and ’03 (yellow) angle gathers

Even though the Tarbert reservoir is not structurally high at this particular well, it is valid to assume that the Tarbert would be experiencing production effects as the reservoirs are connected by faults that can act as a baffle. The effect that we witness in the AVO analysis is due to the progression of water/brine into the reservoir, displacing hydrocarbons and moving the oil water contact up

CONCLUSION

Detailed AVO analysis of three wells cutting across the major reservoirs has been carried out in the G-field. The analysis involves in creating a synthetic model to infer the amplitude responses observed at a particular reservoir horizon. Four types of fluid model substitution were also created; pure brine, pure oil, pure gas and brine mix (70% Brine, 20% Gas and 10% Oil). Significant amplitude changes which correspond primarily to the production effects can be seen in the Tarbert reservoir compared to the Statfjord and Cook reservoirs.

Conclusively, the AVO method is useful for identifying the presence of different fluids throughout the reservoir and that further analysis across the entire area affected by production would be beneficial in mapping fluid changes in the G- field that could then be utilised in improved reservoir management.

Acknowledgements
We wish to acknowledge Stat Oil Company, Norway for providing the data, the interpreting softwares and also to Imperial College London for allowing its use as part of the M.Sc coursework.

REFERENCES

[1] Norwegian Petroleum Directorate, **2012**. *Norwegian Petroleum Directorate's Fact Pages.* [online] Available at < http://www.npd.no/engelsk/cwi/pbl/en/field/all/43686.htm> [Accessed 10 March 2012].
[2] Fossen, H., and Hesthammer, J., **1997**. *Structural Geology of the G- Field, northern North Sea*. In M.P. Coward, H. Johnson, T.S. Daltaban (Eds.), Structural Geology in Reservoir Characterization (pp. 213–261), Geological Society of London Special Publication, Vol. 127
[3] Landro, M., Solheim, O.A., Hilde, E., Ekren, B. O. & Stronen, L. K., **1999**. *Petroleum Geoscience*, Vol. 5, 1999, pp. 213-226
[4] Castagna, Batzle and Kan, **1993**. Rock physics: the link between rock properties and AVO response,Offset Dependent Reflectivity: Theory and Practice of AVO Analysis, Castagna and Backus, pp. 152-154
[5] Castagna, J.P. Batzle, M.L. and Eastwd, R.L. **1985**, *Geophysics* 50, 571-581.
[6] Mavko, G., Mukerji, T. & Dvorkin, J., **2003**. *The Rock Physics Handbook: Tools for Seismic Analysis of Porous Media*. Cambridge University Press.
[7] Gassman, F., **1951**, *Geophysics*, 16, 673-685.
[8] Aki, K., and Richards, P.G., **1980**, Quantitative seismology, Theory and methods, Volume 1. W.H.Freeman and Company.
[9] Rutherford, S. R. and Williams, R. H., **1989**, *Geophysics*, **54,** 680-688

.